### **OPEN ACCESS**



# An Efficient Method for Fitting Radiation-mediated Shocks to Gamma-Ray Burst Data: The Kompaneets RMS Approximation

Filip Samuelsson, Christoffer Lundman, and Felix Ryde <sup>1</sup>Department of Physics TH Royal Institute of Technologyand The Oskar Klein Centre E-10691 Stockholm Sweden; filipsam@kth.se The Oskar Klein CentreDepartment of AstronomyStockholm UniversityAlbaNova, SE-10691 StockholmSweden Received 2021 July 23; revised 2021 October 7; accepted 2021 October 24; published 2022 January 26

#### Abstract

Shocks thatoccur below a gamma-ray burs(GRB) jet photosphere are mediated by radiatios radiationmediated shocks (RMSscould be responsible forshaping the promptGRB emission. Although well studied theoretically,RMS models have not yet been fitted to data owing to the computational cost of simulating RMSs from first principles. Here we bridge the gap between theory and observations by developing an approximate method capable of accurately reproducing radiation spectra from mildly relativistic (in the shock frame) or slower RMSs, called the Kompaneets RMS approximation (KRA). The approximation is based on the similarities between thermal Comptonization of radiation and the bulk Comptonization that curs inside an RMSWe validate the method by comparing simulated KRA radiation spectra to first-principle radiation hydrodynamics simulations, finding excellent agreement both inside the RMS and in the RMS downstream. The KRA is then applied to a shock scenario inside a GRB jet, allowing for fast and efficient fitting to GRB data. We illustrate the capabilities of the developed method by performing a fit to a nonthermal spectrum in GRB 150314A. The fit allows us to uncover the physical properties of the RMS responsible for the prometrission, such as the shock speed and the upstream plasma temperature.

Unified Astronomy Thesaurus concepts: Gamma-ray bursts (629)

#### 1. Introduction

The launching, propagation, and collimation of a highly supersonic jetunavoidably lead to immense shock formation inside the jet and its surroundings (seee.g., López-Cámara inside gamma-ray burst (GRB) jets are mediated by radiation. Such radiation-mediated shocks (RMS&) the jet with hot, nonthermal radiation, which is advected toward the jet photospherewhere it is released. The released spectra will range from strongly nonthermal to thermal, depending on before reaching the photosphere or not.

GRBs are observed to have strong spectraevolution, in terms of both peak energy (Golenetskii et aps and shape (e.g., the width of the spectrum; Wheaton et al. 1973). In around one-quarter of GRB pulses, the narrowest, timeresolved spectrum is consistent with a thermal spectrum, which strongly suggests that the whole pulse is of a photosphericorigin (Yu et al. 2019; Acuner et al. 2020, Dereli-Béguéet al. 2020; Li et al. 2021). It is plausible, therefore, that the wider, nonthermal spectra in such pulses have undergone subphotospheric dissipation (Rees & Mészái 2005; Ryde et al. 2011). Even though RMSs are a natural cause tions. In Section 2, we construct an approximate, but very fast, of this dissipation, so far RMS models have not been fitted to the data3.

Currently, these 1D simulations are not fast enough to build a table model of simulated RMS spectra overthe relevant parameterspace, which is an efficient way to test models against data. However, model testing is of crucial importance to further develop our understanding of the prometmission in GRBs. With this motivation, in this work we explore an method called the Kompaneets RMS approximation (KRA). The approximation is based on the strong similarities between bulk Comptonization of radiation inside an RMS and thermal Comptonization of radiation on hotelectrons, the latter being photospheric models including dissipation to the data. However, their assumed energy dissipation mechanism was a firm of the data. However, their assumed energy dissipation mechanism was a firm of the data. priate to use for mildly relativistic (and slower), optically thick RMSs. We validate the KRA by comparing simulated radiation spectra to those produced by the full radiation hydrodynamics simulations, finding excellent agreement. The KRA is then applied to a minimal model of a shock inside a GRB jet in Section 3, which generates synthetic photospherics pectra,

Original content from this work may be used under the terms of the Creative Commons Attribution 4.0 licence. Any further distribution of this work must maintain attribution to the author(s) and the title of the work, journal citation and DOI.

The main reason for this is that RMSs are expensive to simulate from first principles. RMSs have previously been considered in one spatialdimension (Levinson & Bromberg 2008; Nakar & Sari 2012; Beloborodov 2017; Ito et al.018; et al. 2013, 2014; Gottlieb et al. 2019). Shocks that occur deep 2020; Levinson & Nakar 2020; Levinson 2020; Lundman & Beloborodov 2019; Ito et al. incide gamma ray burst (GPR) into are mediated by radiation. Beloborodov 2021). The 1D simulations illustrate the main features of the nonthermal RMS radiation expected inside GRB jets: a broad power-law spectrum for up to mildly relativistic shocks (that have relative relativistic speed between the up- and whether the radiation has had time to thermalize via scatterings speed of light c and γ is the Lorentz factor), while faster shocks downstreams of  $\beta\gamma$   $\Box$  few, where  $\beta$  is the speed in units of have more complex spectrashapes owing to Klein-Nishina effects, anisotropic radiation in the shockand photon-photon pair production. Once advected into the downstream, the RMS spectrum gradually thermalizes through scatterings.

energy dissipation mechanism was different.

accounting for both adiabatic cooling and thermalization of the photon distribution. The KRA simulations are about four orders of magnitude faster to run than the corresponding 1D simulations, allowing for table model construction. As an illustration of the model capabilities, we use the table model to perform a fit to the prompt emission of GRB 150314A in Section 4. We conclude by summarizing and discussing our results in Section 5.

#### 2. The Kompaneets RMS Approximation

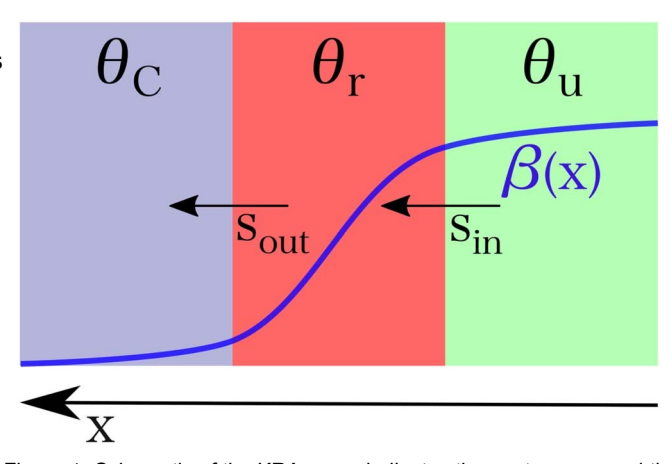
In this section, we develop the KRA and compare the resulting spectra to full-scale pecial relativistic RMS simulations in planar geometry. The approximation is valid for RMSs where the photons inside the shock do not obtain energies exceeding the electron rest mass energy, as the transfer probletingure 1. Schematic of the KRA: green indicates the upstream zoned the then becomes more complicated, including Klein-Nishina scattering effects, anisotropy, and γγ-pair production. This typically corresponds to shocks thate mildly relativistid or slower, inside plasma where the downstream radiation pressurgue line is a rough indication of the velocity profile, B(x), across a real RMS. dominates over the magnetic pressure.

As is appropriate for RMSs inside GRB lets, the RMS is assumed to be photon rich (Bromberg et al. 2011), i.e., the photons inside the RMS are mainly supplied by advection of upstream photons opposed to photon production inside the RMS and in the immediate downstream. The RMS is also assumed to be in an optically thick region, which is appropriate not hold for shocks that dissipate most of their energy close to energy  $\dot{o}$  is given in units of electron restnass,  $\dot{o} = hv/m_ec^2$ , the photosphere such shocks require full radiation hydrodynamics simulations. We note that Blandford & Payne (1981) showed that the shape of a photon spectrum traversing Aò is the energy gain in a scattering for a photon with initial photon-rich, nonrelativistic RMS can be obtained analytically. Although their analytical calculation is impressive it ignores photon energy losses due to electron recoil. The photon spectrum, therefore, lacks a high-energy cutoff, which makes i accurate only for soft spectra where the bulk energy is not carried by the high-energy photons. Due to this limitation, their across the shock). The  $d\beta/d\tau$  profile is self-consistently solution is not applicable here.

# 2.1. Bulk Comptonization inside the RMS

comparison to full RMS simulations shows that the approximation is valid also for mildly relativistic shocks with  $v\beta \square$  few (see also Section 2.4).

is greater than the outgoing speed of the downstretending to a speed gradient inside the shockhe photons that diffuse energy by scattering on fast electrons. If the photon mean free per scattering is balanced by energy losses due to electron path is λ, the velocity difference of the plasma over a scattering ecoil, which occurs when Δò/ò ≈ ò. This gives a maximum length is  $\square \lambda(d\beta/dx) = d\beta/d\tau$ , where x is the spatial coordinate photon energy inside the shock of and  $d\tau = dx/\lambda$  measures the optical depth along the xcoordinate. Doppler-boosting the photon to the frame of the scatterer, performing a scattering, and averaging over the



RMS zone, and purple the downstream zonen each zone, photons interact with a population of thermal electrons with an effective temperature,θ. Dissipation occurs in the RMS zone by prescribing the electrons a high temperature,  $\!\theta\!\!\!/\;\theta$   $_{u}\!\!\!.$  The zones are connected via source terms, s. The overlaid where x is the spatial coordinate.

scattering anglesone finds a relative energy gain of

$$\frac{\mathbb{D}\,\mathbb{I}}{\mathbb{I}} \gg \frac{1}{3} \left| \frac{db}{dt} \right| \tag{1}$$

deep below the photosphere. The approximation will therefore per scattering, e.g., a first-order Fermi process. Here the photon where h is Planck's constant v is the photon frequency. Equation (1) is valid for a relative energy gain  $\Delta \hat{o}/\hat{o} < 1$ , where energy ò. Note that dβ/dτ is a local quantity that changes continuously across the RMS transition region and vanishes in the far up- and downstreams, where the plasma velocity is constant(see Figure 1 for a schematic of the velocity profile determined by the radiation feedback onto the plasma:the photons gain precisely the available kinetic energy such that the Rankine-Hugoniot shock jump conditions are satisfied.

Since plasma is advected through the RMS, so are the The following treatment assumes a nonrelativistic shock, butphotons that scatter inside the plasnidowever, photons also diffuse within the flow, and a fraction of the photons will stay inside the RMS much longer than the advection time across the RMS, accumulating more scatterings and therefore more In the shock rest frame, the incoming speed of the upstreamenergy. As is always the case when both the probability of escaping the shock and the relative energy gain per scattering, Δò/ò, are energy independent, a power-law spectrum develops. inside the RMS speed gradient directly tap the incoming kinetic The power law extends up to energies where the energy gain

$$\square_{\mathsf{max}} \, \mathsf{v} \, \left\langle \frac{\mathsf{D} \, \square}{\square} \right\rangle, \tag{2}$$

where the brackets on the right-hand side indicate a weighted average across the shock.

The exact expression for aD 1/1 n is difficult to determine energies in the up- and downstreams, respectively, and the four-velocity of the upstream evaluated in the shock rest frame,

We illustrate this point later with a shock simulation that has an upstream four-velocity of  $\beta y = 3$ .

Lundman & Beloborodov (2021) show the evolution of a mildly relativistic RMS that reaches the edge of neutron star merger ejecta. The shock evolution from first principles. With  $\mathbb{T}_u$  and  $\mathbb{T}_d$  as the average photon is complex: the radiation begins leaking ahead of the showkhile a forward collisionless shock and a reverse collisionless shock are formed at the photosphere.

we empirically find in Appendix A that

$$\frac{D}{\mathbb{I}} \right) \gg \frac{(b_U g_I)^2 \ln(\mathbb{I}_d / \mathbb{I}_U)}{X}, \tag{3}$$

with  $\xi$  = 55 is a good approximation across the relevant shock parameter space. Although Equation (3) contains the relativistic four-velocity, it is only valid while áD \$\mathbb{0} / \mathbb{0} \tilde{n} \times \mathbb{0}\_{max} \mathbb{0} \tag{1}.

### 2.2. Modeling an RMS as Thermal Comptonization

The energy gain process described in Section 2.1 looks strikingly similar to thermal Comptonization on hotelectrons (see, e.g., Rybicki & Lightman 1979). Consider a hot cloud of nonrelativistic electrons at a constant temperature $\theta = kT/$  $m_e c^2 = 1$ , where k is the Boltzmann constant and T is the temperature, with injection of low-energy photons ( $\grave{o} = \theta$ ) into The low-energy photons will gain a relative energy per scattering of  $\Delta \dot{o}/\dot{o} \approx 4\theta$ , and the energy gain continues until balanced by recoilosses at  $\square_{max}$  » D  $\square/\square$  » 4q. Such Comptonization is described by the Kompaneets equation with a source term s for the photon injection and escape from the cloud

$$t_{\rm sc} \left( \frac{\P^n}{\P^t} \right) = \frac{1}{\mathbb{I}^2} \frac{\P}{\P^{\parallel}} \left[ \mathbb{I}^4 \left( \frac{\P^n}{\P^{\parallel}} + n \right) \right] + S, \tag{4}$$

where  $t_c = \lambda/c$  is the Thompson scattering time and n is the photon occupation number.Stimulated scattering (∝n²) has been omitted in Equation (4)as this effectis insignificant as long as the occupation number is small, = 1, which is true for the nonthermal emission considered here.

Motivated by the similarities between the two systemsur aim is to constructan approximate RMS modebased on the Kompaneets equationThe plasma is split into three discrete zones: the upstream zone, the RMS zone, and the downstream umber inside the RMS zondn this scenario, one can show zone. The time evolution of the radiation spectrum inside each (e.g., Rybicki & Lightman 1979) that the steady-state solution zone is computed using the Kompaneets equaticach zone connected via source terms. A schematic of the KRA is shown law distribution,  $n \propto \dot{o}^{-\alpha}$ , with a = 3/2 [  $(9/4 + k/q)^{1/2}$ ]

The upstream zone feeds thermaladiation into the RMS zone, which passesradiation onto the downstream zone. Dissipation occurs only inside the RMS zone. This is achieved by prescribing an effective electron temperatorres  $\frac{1}{2}$   $\boxed{1}$ found from Equation (3) as

$$4q = \frac{(b_u g_l)^2 \ln(\mathbb{I}_d/\mathbb{I}_u)}{\chi}.$$
 (5)

The subscript here and henceforth denotes quantities in the RMS zone, and the subscripts u and d wilbe used to denote RMS zone, and the subscripts u and d wilbe used to denote spectrum, with larger values of y<sub>r</sub> giving harder slopes. The quantities in the upstream and downstream zones, respectively value of y<sub>r</sub> in the KRA is chosen such that the average energy gain per scattering in the RMS zone mimic those of a real RMS. By matching how long photons stay in the shock such that the average downstream energies in the two systems Appendix A. become equalthe evolution of the photon distribution in the KRA will closely match that of a real shockThis is achieved by using appropriate source terms (see Section 2.3).

The up- and downstream zonesdo not dissipate energy. Therefore, the temperaturesinside these zones equal the

radiation Compton temperature Q, defined as the electron temperature with which there is no net energy transfer between the photon and electron populations is given by

$$4q_{\mathbb{C}} = \frac{\grave{O}^{\parallel 4n} d_{\parallel}}{\grave{O}^{\parallel 3n} d_{\parallel}},\tag{6}$$

where the integrals are taken overall photon energies. The upstream temperature of the radiation, is a free parameter of the model, but the downstream Compton temperature is not a free parameter, as it is determined by the upstream temperature and the amount of dissipation in the shock. The nonthermal radiation that streams from the RMS zone is accumulated in the downstream zonewhere it gradually thermalizesvia scatterings. The downstream zone contains alphotons that passed the cloud and an escape probability that is energy independent through the RMS zone, and the degree of thermalization of the radiation inside the downstream zone increases with time.

#### 2.3. The KRA Source Terms

The three zones in the KRA are coupled by source terms. Denoting the source of photons that stream into the RMS by s and the source that streams out of the RMS bytsone gets

$$S_u = -S_{in}, \tag{7}$$

$$S_r = S_{in} - S_{out}, \tag{8}$$

$$S_d = S_{\text{out}}. (9)$$

The probability for a photon to escape the RMS into the downstream is independent of the photon energy. Thus,  $s_{\text{out}} = kn_r$ , where k is a constant and  $n_r$  is the occupation to the Kompaneets equation inside the RMS zone is a power-In analogy with Rybicki & Lightman (1979), we identify the RMS zone y-parameter as  $\neq 4\theta_r/k$ . Therefore,

$$S_{\text{out}} = \left(\frac{Aq}{y_r}\right) n_r. \tag{10}$$

The RMS zone y-parameterdetermineshow much time photons spend inside the shock; therefore, it is a measure of the average photon energy gain inside the RMAs such, y<sub>r</sub> sets the hardness of the nonthermal spectrum that is injected into the downstream. A value of  $y_r = 1$  corresponds to a flat  $vF_v$ Equation (5) assures that the maximum photon energy and the downstream photon energy obtained equals that of a real RMS. The full conversion between the parameters that ecify the RMS and the corresponding KRA parameters shown in

We use a Wien distribution for the upstream radiation, hich is a Planck spectrum with nonzero chemical potential.

That is, high-energy photons preferentially lose energy as they scatter, while low-energy photons gain energy he net effect is to gradually thermalize the photon distribution, while keeping the average photon energy constant.

Requiring that the photon number inside the RMS zone is conservedone finds from Equation (8)

$$S_{\text{in}} = \left(\frac{Aq}{y_r}\right) \left(\frac{\grave{o}^{2n_r d}}{\grave{o}^{2n_u d}}\right) n_u, \tag{11}$$

where the integrals are again taken over all photon energies.

# 2.4. Estimating the KRA Upper Speed Limit

The energy gain inside the RMS qualitatively changes when the relative energy gain per scattering, Δò/ò, becomes comparable to unity. This is because the upper photon energy inside the shock is  $_{max}$  » D []/[], and the radiative transfer is different for such high-energy photons.n particular, Klein-Nishina effects modify the scattering cross section, and vy-pair production is triggeredFurthermoreshocks with such a high energy gain per scattering wilhave a narrow width (comparable to a few photon mean free paths), which makes the radiation anisotropic. The KRA is therefore limited to modeling The radshock code is a special relativistic, Lagrangian shocks with  $\Delta \hat{o}/\hat{o} \square$  1This corresponds to (see Equation (3))

$$(b_{u} g_{l})^{2} \mathbb{I} \frac{X}{\ln(\mathbb{I}_{d}/\mathbb{I}_{u})}, \tag{12}$$

with  $\xi \approx 55$ .

The ratio of average downstream to upstream photon energies can vary significantly buenters Equation (12) only as a logarithmic factor. For a typical energy ratio of  $\mathbb{I}_u/\mathbb{I}_u=10^2$ , one gets an upper velocity limit of  $\beta_u\gamma_u\approx 3.5$ . Thus, the KRA is expected to be applicable to shocks with  $\beta_u \gamma_u \square 3$ , with the exact value only marginally dependent on the shock parameters.

### 2.5. Quasi-thermal RMS Spectra

thermal if the energy dissipation per photon is either very low or very high. In the former case the upstream photon distribution is largely unaltered, while in the latter case the photons gain so much energy thathey pile up in a thermal Wien distribution around<sub>max</sub> (i.e., saturated Comptonization). In both cases, the radiation relaxes to a near-thermal distribution after a few scatterings in the downstream, at which point the information from the shock is all but lost. When fitting to data, such shocks are almostidistinguishable from each other and from outflows where no dissipation occurred. As such, they are less interesting from an observational perspective.

Shocks with small photon-to-proton ratios,/n p, where n and n<sub>p</sub> are the photon and proton number densities, respectively, tend to have more thermal-like spectra inside the RMS. This is because the average downstream photon energy is inversely proportional to the photon-to-proton ratio (i.e., more photons sharing the same shock kinetic energy), while the maximum photon energymax is proportional to the logarithm of (see Equation (3)). Thus, as the photon number it is not obvious a priori what part should be compared to the shrinks, dincreases faster than, until the spectrum appears quasi-thermal with  $\mathbb{I}_d \sim \mathbb{I}_{\text{max}}$ .

For  $\mathbb{I}_{\mathcal{U}} \square \mathbb{I}_{\mathcal{U}}$ , the average downstream photon energy is

where m is the proton mass. Equating to  $\mathbb{I}_{max} \gg D \, \mathbb{I} / \, \mathbb{I}$  and solving for n<sub>v</sub>/n<sub>p</sub>, one gets

$$\frac{n_g}{n_p} \gg \frac{g_l - 1}{(b_l g_l)^2} \frac{m_p}{m_e} \frac{\chi}{\ln\left(\frac{\pi}{l_l}/\frac{\pi}{l_l}\right)}.$$
 (14)

Consider the limit  $\beta_{ij} = 1$ , which gives  $(q_i - 1)/(b_{ij} q_j)^2$  » 1/2. With  $\xi = 55$  and a typical energy ratio of  $\mathbb{I}_u / \mathbb{I}_u = 10^2$ . one finds a critical photon-to-proton ratio  $\rho fm_b \approx 1.1 \times 10^4$ . Shocks that have photon-to-proton ratios close to this value will result in quasi-thermal radiation spectra. Below, we illustrate this fact with a simulation that has n<sub>v</sub>/n<sub>n</sub>≈

# 2.6. Comparing the Kompaneets RMS Approximation to Full **RMS** Simulations

In this subsectionwe will compare the spectrum inside the RMS and downstream regions as computed by the two codes radshock and Komrad, the latter implementing the KRA. radiation hydrodynamicscode (Lundman et al. 2018). The radiation field is computed using the Monte Carlo method, which self-consistently connects to the hydrodynamicsvia energy and momentum source term\she RMS is set up by smashing plasma into a wall boundary condition and allowing the code to relax into an RMS that propagates steadily away from the wall. For the case of a thermal upstream radiation spectrum, the RMS solution is fully specified by three parametersThese can be taken to be the temperature of the upstream radiation,  $\theta_{\text{u}}, \ \text{the speed of the upstream plasma}$ relative to the shock,  $\beta$  and the photon-to-proton ratio,  $/n_p$ , inside the upstream (Lundman et 2018).

Komrad implements the KRA described in the previous subsections evolving the radiation in the RMS zone and the downstream zoneusing Kompaneets solvers (e.chang & The radiation in the downstream of an RMS becomes quasidescribe the RMS in Komrad: the temperature of the upstream photons,  $\theta_{u, K}$  (where the subscript indicates Komrad), the effective electron temperature inside the RMS zonæned the Compton y-parameter the RMS zone, y<sub>r</sub>. As mentioned above, the conversion from the KRA parameters to the corresponding RMS parameters is given in Appendix A.A. nontrivial point is that the two codes will have somewhat different upstream temperatures. This is because plasma compression inside the RMS willncrease the internælnergy density and shift the upstream spectral peakd no analog to this compression exists for the KRA.

> A simulation is fully specified by the three shock parameters and the total simulation time tt. The simulation time affects the degree to which the downstream has been thermalized. highlight the similarities between the downstream spective. do not include the radiation produced during the initiaRMS formation. This is becausethe formation of the shock is different between the simulations. Therefore, the simulation time starts when the RMS is already in steady state.

> The RMS transition region in radshock is continuous, and RMS zone in Komrad. For the comparison, we chose the radiation in radshock that is located at the point where the shock has just finished dissipating all incoming energy, as this

The upstream zone has no need for a Kompaneets solver, as the radiation is assumed to be thermal and the shape of the spectrum is known analytically.

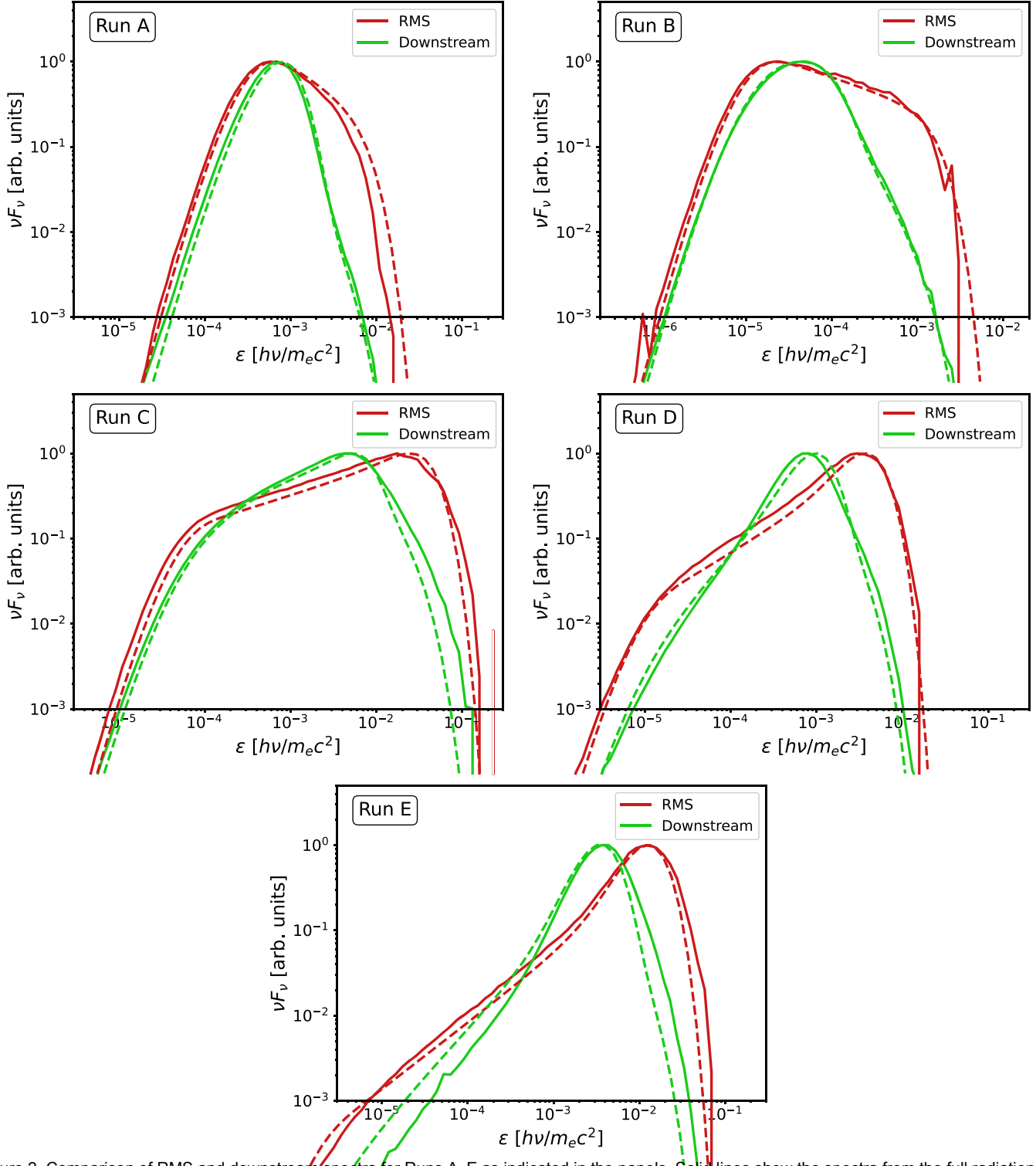


Figure 2. Comparison of RMS and downstream spectra for Runs A–E as indicated in the panels. Solid lines show the spectra from the full radiation hydrodynamics code radshock, and dashed lines show spectra from the KRA code Komrathe parameter values for the runs are given in Tables 1 and 2.

represents the spectrum that injected into the downstream. This location is determined as the point where the average photon energy has reached its downstream value plasma that has passed through this location after the start of the simulation time belongs to the downstreamt the end of the simulation, the radiation inside the downstream is collected an parameter space, resulting in differently shaped radiation its spectrum computed.

Figures 2 and 3 show the results of six different shock simulations, labeled Runs A-F. The Komrad parameters for the six runs are shown in Table 1, and the radshock parameters are found in Table 2.The simulation parameters were chosen to test the KRA in different regions of the shock spectra inside the shock he Komrad parameters for the six

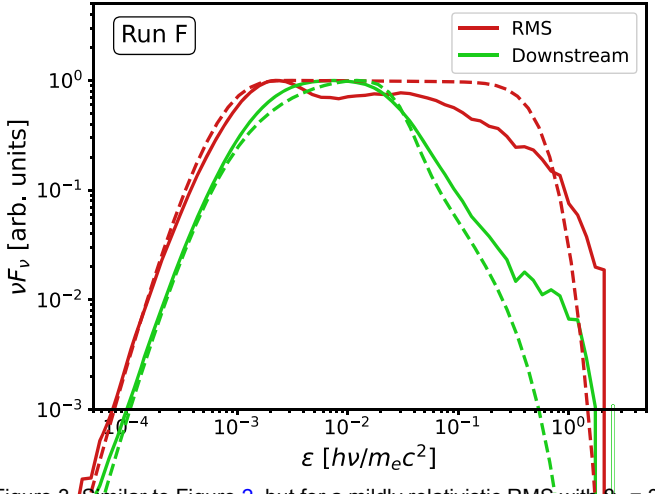


Figure 3. Similar to Figure 2, but for a mildly relativistic RMS with 3 = 3(Run F). The RMS width is only a few optical depths wideand photons can easily diffuse in and out of the shock. Thus, the comparison to a discrete, well-spectrum is often given little weight in the fitting process owing defined zone in Komrad becomes less accuraten the downstream,Klein-Nishina effects suppress the cooling of the highest-energy photons. Paramete values for the run are given in Tables 1 and 2.

Table 1 Komrad Simulation Parameters

Run	t/t sc	θ <sub>u, K</sub>	$R \equiv \theta_r/\theta_{u, K}$	<b>y</b> r
Α	5 × 10 <sup>3</sup>	1.05 × 10 <sup>-4</sup>	15.3	0.56
В	1.5 × 10⁴	3.35 × 10 <sup>-6</sup>	110	0.70
С	320	1.73 × 10 <sup>-5</sup>	522	1.58
D	5 × 10 <sup>3</sup>	3.35 × 10 <sup>-6</sup>	325	2.97
E	2834	$6.04 \times 10^{-7}$	5644	5.6
F	80	2.51 × 10 <sup>-4</sup>	403	0.99

Table 2 radshock Simulation Parameters

Run	t/t sc	$\theta_{u}$	$\beta_{\text{u}}$	n <sub>γ</sub> /n <sub>p</sub>
A	5 × 10 <sup>3</sup>	6.13 × 10 <sup>-5</sup>	0.490	5.47 × 10 <sup>5</sup>
В	1.5 × 10 <sup>4</sup>	1.89 × 10 <sup>-6</sup>	0.224	1.70 × 10 <sup>6</sup>
С	320	8.86 × 10 <sup>-6</sup>	0.610	$4.82 \times 10^{5}$
D	5 × 10 <sup>3</sup>	1.75 × 10 <sup>-6</sup>	0.228	9.00 × 10⁴
E	2834	3.14 × 10 <sup>-7</sup>	0.303	4.12 × 10⁴
F	80	1.1 × 10 <sup>-4</sup>	0.949	10 <sup>6</sup>

runs are calculated from the corresponding radshock parameters using the method described in Appendix A.he only free parameter in the conversion is  $\xi$  from Equation (3). All Komrad runs are made with  $\xi = 55$ , as we empirically found that this value gave good agreement across the parametaleep enough to launch two shocks he shocks propagate in

In Figure 2, Runs A–E are shown in five different panels. highlighting the close analogy between bulk and thermal Comptonization. We conclude that the KRA can accurately capture the RMS radiation physics.

In Figure 3, we show the spectra for Run F, which is a mildly relativistic shock with upstream speed  $_{u}$   $_{u}$  = 3 in the shock rest frame. The KRA neglects relativistic effects such as Klein-RMS can transform into a pair of collisionless shocks athe Nishina suppressionand pair production. Furthermore, as shown in, e.g., Ito et al. (2018), anisotropy starts to become important when the shock becomes relativistic. However, Komrad can still capture the behavior mildly relativistic

shocks as long as the photon energies inside the RMS do not exceed the electron restmass, i.e., as long as Imax I 1 as discussed in Section 2.4.

In this run, the relative energy gain per scattering is close to unity, and the shock is only a few Thomson optical depths wide in the radshock simulation. Hence, photons have a high probability of diffusing in and out of the different regions, and there are no sharp "zone boundaries" in radshock. Therefore, the comparison to a discrete RMS zone in Komrad is less accurate. Furthermore. Klein-Nishina suppression startsto become important This can be seen in the high-energy tail of the photon distribution in the downstream. The high-energy photons in radshock have cooled less than those in Komrad. due to their lower scattering cross section. However, this effect will likely be unimportant when the KRA is fitted to actual data, as radiation with ò \( \simeq 1 \) has time to downscatter to lower energies before reaching the photosphereyen with Klein-Nishina suppressior Furthermore the high-energy part of the to the lower photon counts at high energies in the GBM energy channels (Yu et al. 2019). Overall the approximation is surprisingly accurate even in this case when  $\beta_{11}y_{11} = 3$ , especially in the downstream zone, which contains the radiation that will later be observed. This indicates that any anisotropy of the radiation field within the shock does not have a major impact on the shape of the spectrum in this callete conclude that the limit of the KRA is when  $\square_{\max}$  »  $D \square / \square \gg 4q$  starts to approach unity.

### 3. Applying the Kompaneets RMS Approximation to a **GRB Jet**

RMSs come with a variety of dynamical behaviors. Explosions, such as supernovaegenerate an outward-going shock wave. The shock wave propagates through the star until it either breaks out of the stellar surface (i.e., the photosphere) or dissolves as the downstream pressure becomes too small, due to the limited explosion energy budget. A different dynamical behavior is seen in recollimation shocks, which arise as the jet propagates in a confining medium. Such shocks can be approximately stationary with respect the star and might therefore never break out. However, the radiation that is advected through the recollimation shock is energized, and the emission released athe photosphere can be nonthermalet another behavior is seen in shocks that arise owing to internal collisions of plasma inside the jet. When two plasma blobs collide, the plasma in between the blobs is compressed, increasing the pressure adiabatically until the pressure profile is opposite directions into the two colliding blobs while sharing a causally connected downstream regionSuch shocks cease The spectra produced by the two codes are remarkably similar when they have dissipated most of the available kinetic energy in the two blobs. The time it takes the shocks to cross the blobs is roughly a dynamical time (as they cross the causally connected jet ejecta).

> Dynamical effects on the shock structure are important if the shock reaches the jetphotosphereFor instance, part of the point of breakout when the photons mediating the shock start to leak out toward infinity (Lundman & Beloborodov 2021). The KRA is not able to handle such dynamical effects. On the other hand, the KRA is well suited for simulating plasma thatis

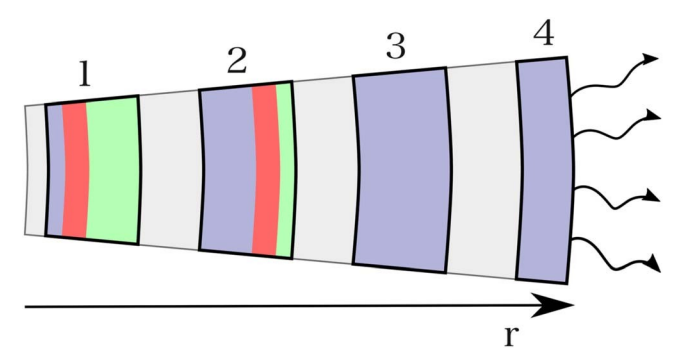


Figure 4. Schematic showing four stages in the evolution of the minimal shock Compton scattering (e.g.promberg et al. 2011; Lundman & model from left to right. Green, red, and purple indicate the upstrear RMS, and downstream zonesespectively At some optical depth T<sub>i</sub> (small r), the shock is initiated. Photons starto diffuse through the shock region and gain energy. The photons that pass through the RMS are collected in the downstream region, which gains more and more photons (stages 1 and 2). When the RMS has crossed the upstream it dissolves leaving only the downstream (stage 3). The photons in the downstream continue to scatter un they are released at the photosphere (stage 4).

shocked while still being optically thick and then advected toward the jet photosphere, where the emission is later released.

# 3.1. A Minimal Subphotospheric Shock Model

One shock scenario that can be modeled by the KRA is the collision inside the jet of two blobs of similar mass and density but different speeds. This is a minimal scenario with few free parameters More complex models with addition abarameters can be considered in the future, if the current model fails to fit prompt GRB data. In Appendix B we compute the speed of the the Kompaneets equation can be written as two shocks, the energy dissipated, nd the radius at which the shocks have finished dissipating most of the available energy. For blobs of similar properties (i.e., similar mass and density), we show that also the properties of the shocks are similan. that case, only one of the two shocks has to be explicitly simulated, and the number of model parameters is keptat a minimum.

The KRA is valid for shocks where Δò/ò □ tas discussed in Section 2.4. In Appendix B we translate this limit to jet quantities in the context of internal shocks. It corresponds to a  $\tau = \sigma_T n_e r/\Gamma$  is the optical depth of the jet (not to be confused Lorentz factor ratio of  ${/\!\!\!\!/}\Gamma_1 \square 30$ , where  ${/\!\!\!/}$  and  ${/\!\!\!\!/}\Gamma_1$  are the lab frame Lorentz factors of the fast and slow blobespectively. As an example,  $\Gamma$ = 50 and  $\Gamma$ <sub>2</sub> = 1000 produce shocks that the KRA can accurately model.

A schematic illustration of the minimal shock model at four different stages of its evolution is shown in Figure 4. In the first  $t = r/\Gamma c$ . stage, the two blobs have recently collided. The RMS has started to propagate into the upstream, and a few photons haveor adiabatic cooling of the spectrum. In the optically thick had time to diffuse into the downstreamn the second stage, the shock has almost crossed the upstreamThe shock has finished crossing the upstream and dissolved in the third stagespectrum is preserved. When the photons start to decouple stage shows the radiation being released the photosphere. Each of the three zones accounts for thermalization of the photon spectrum via scatterings and adiabatic cooling.

The time over which shocks dissipate their energy is not free parameter; it should be found self-consistently from g., hydrodynamical simulations. However, the shock crossing time is always comparable to the dynamicatimescale of the jet, which corresponds to a doubling of the jetadius. Therefore, we let the KRA dissipate energy over doubling of the jet

radius in our shock modelThis also corresponds to a halving of the optical depth as we consider the case of a conical outflow. After the shock stops dissipating the downstream plasma containing the shocked radiation is advected toward the photosphere, while it gradually thermalizes through scatterings and cools adiabatically. The simulation ends when the shocked radiation reaches the photosphere.

As mentioned above, we omit photon production by the plasma (i.e., the shock is photon rich). This is a valid assumption, as the advected flux of upstream photons already existing inside the GRB jet is much larger than the number of photons produced by bremsstrahlung ordouble Beloborodov 2019). Photon production will occur in the downstream, but the timescale for such production is long; the photon spectrum thermalizes into a Wien spectrum via scatterings long before photon production acts to modify the Wien spectrum into a Planck spectrum. As shown by Levinson il(2012) photon production has time to modify the spectrum if the shock occurred at optical depths of ~5.10n that case, the radiation will have lost essentially allits energy to adiabatic expansion before reaching the photosphere and is therefore of

# 3.2. KRA Implementation in Spherical Geometry

A conical jet appears locally as spherically symmetriche Kompaneets equation inside a steady-state, spherical relativistic outflow (with outflow bulk velocity  $\beta \rightarrow 1$ ) is given by Equation (3) of Vurm & Beloborodov (2016). With the assumptions of a constantfulk Lorentz factor  $\Gamma$ , no induced scattering (n = 1), and no emission or absorption of photons,

$$\frac{\P}{\P^{\overline{\Gamma}}}(\overline{\Gamma^{2}}) = \frac{1}{\mathbb{Q}^{2}} \frac{\P}{\P \mathbb{Q}} \left\{ \frac{\mathbb{Q}^{4}}{\overline{\Gamma^{2}}} \left[ q \frac{\P(\overline{\Gamma^{2}})}{\P \mathbb{Q}} \right] + (\overline{\Gamma^{2}}) \right\} + \frac{2}{3} \frac{\mathbb{Q}^{3}(\overline{\Gamma^{2}})}{\overline{\Gamma}} \right\} + S.$$
(15)

where  $r = rR_{ph}$  is a normalized radius and R the radius of the photosphere. The normalized radius  $eq\overline{u}$  als 1/t, where with the optical depth of the RMS), with being the Thomson cross section and n<sub>a</sub> the electron number density. The comoving time coordinate in the Kompaneetsequation has here been rewritten into a lab frame radiacoordinate (using

The last term in the curly brackets of Equation (15) accounts regime, this causes the average energy of the photon distribution to decrease as  $F^{-2\beta}$ , while the shape of the with all photons accumulated in the downstream, and the fourthclose to the photosphere (τ □ 1), the evolution changes and the idealized cooling of  $\overline{r}^{-2\beta}$  is no longer valid (Pe'er 2008; Beloborodov 2011). To account for this, we numerically stop the cooling at an optical depth of  $\tau = 3$ . The total adiabatic cooling of the photon distribution is then similar to that a

The Kompaneets solver method described in Chang & Cooper (1970) with a small grid size is not directly applicable here anymoresince no stationary solution to the Kompaneets equation exists when adiabatic cooling is included. However, increasing the energy grid size assures that convergence is obtained.

account (see Beloborodov 2011). Scattering is incorporated until  $\tau = 1$ .

# 3.3. Lab frame Transformation of the Simulated Radiation Spectrum

The simulation outputs the comoving radiation spectrum at the jet photosphereThe simplestapproximate transformation to the lab frame involves multiplying all photon energies by a factor  $\Gamma$  (the Doppler boost for a typical photon), where  $\Gamma$  is thethe combined parameter  $\tau\theta$  determines the amount of Lorentz factor of the downstream zone. Since  $\Gamma$  does not explicitly enter the simulation, it is effectively a postprocessing parameter.

In reality, the radiation spectrum broadens somewheat it decouples from the plasma at the jet photosphere (Pe'er 2008;to a Wien spectrum, in which case the original shock Beloborodov 2010; Lundman et al. 2013). This is because individual photons decouple adifferent angles to the line of sight, which affects their Doppler boostand also at different radii, which affects their energy losses due to adiabatic expansion. These effects are importanto take into account when performing spectrafits to data, specifically to narrow bursts (Ryde et al. 2017). This spectral broadening can be approximately computed in a post-processing stemder the assumption that the jet Lorentz factor  $\Gamma$  is constant at the photosphere. The post-processing calculation is fairly long and parameter on the final spectrum is more clearly seen. will be described in full detail elsewhere.

The Kompaneetsequation without the induced scattering term is linear in the photon occupation number nTherefore, the total photon number of the simulation is also a free parameter, which effectively makes the normalization of the GRB luminosity a post-processing parameter.

### 3.4. New Parameters Based on Parameter Degeneracy

In the case of planar geometry described in Section the KRA has three parameters; **Q**, and y. In the case of a jet, the optical depth of the jet where the shock is initiated; is an photosphericspectrum in the rest frame of the outflow. Additionally, as described in the subsection abovene bulk Lorentz factor  $\Gamma$  and the luminosity, lare two post-processing

set. As long as the product  $_{i}\theta_{r}$ , the ratio  $\theta/\theta_{u}$ , and  $y_{r}$  remain unchanged, the spectral shape in the rest frame of the outflow pulse structure such as the one in GRB 150314A (Yu et al. identical. With the translational freedoms given by  $\Gamma$  and  $\downarrow$ , this becomesdegenerate. Therefore, a more suitable set of parameters  $t\theta = t_i\theta_r$ ,  $R = \theta_r/\theta_u$ , and  $y_r$ . This brings the number of simulation parameters down from four to three, which simplifies the process of table model building.

The degeneracy can be understood as follows agine that  $\tau_i$  is increased by some factor but  $\theta_i$  and  $\theta_i$  are decreased by the same amount. The evolution of the photon distribution with Beloborodov 2019). optical depth is sloweras the energy transfer per scattering is energy in the scattering) or the photon energy (when the photoparameterspace using Komrad within the minimal shock loses energy), both of which have decreased by a factorf. However, the number of scatterings is ftimes larger, so the relative energy transfer is the same, the spectrum evolves the evolution of the whole system is equivalent the shape of the photospheric spectrum is identical but shifted down in

real spectrum where the proper radiation transfer is taken into energy by a factor 7/3, where an additional factor 2/3 comes from the increased adiabatic cooling. The degeneracyin number of scatterings and energy gain pescattering is not unique to our model. Indeed, it is inherent to all jetted RMS models.

> To see how each parameter influences the shape of the released photospheric spectrum, Figure 5 we vary τθ (top panel), R (middle panel), and (bottom panel), while keeping the other parameters constant. The value of the parameter being varied increases from black to red. As can be seen in the figure. thermalization after the shock has finished dissipating its energy. A higher τθ implies a higher number of scatterings and/or higher energy transfer per scattering, leading to a faster thermalization For large  $\tau\theta$  the downstream spectrum relaxes parameters cannot be retrieved. The ratio R/€, bdetermines the separation between the lower and upper cutoff in the spectrum. A large R leads to a long power-law segment in the downstream. The slope of the power-law depends on the Compton y-parametey, which is a measure of how much energy is dissipated in the shock-ligher values of y lead to harder spectra, with  $y_r = 1$  corresponding to a flat  $vF_v$ spectrum. The spectral broadening discussed in Section 3.3 has been omitted in Figure 5, so that the effect of each

# 4. Fitting GRB Data with the Kompaneets RMS Approximation

As a proof of concept of fitting an RMS model to prompt GRB emission datawe present an analysis of a time-resolved spectrum in GRB 150314A. This luminous burst was observed by the Fermi Gamma-ray Space Telescope and its Gamma-ray Burst Monitor (GBM), which covers the energy range of 8 keV-40 MeV.

GRB 150314A is an example of a GRB pulse in which the additional parameter. Together, they determine the shape of the pectrum becomes very narrow during a portion of its duration (Yu et al. 2019). The low-energy photon index,  $\alpha$ , of the Band function (Band et al. 1993) reaches a very large value,  $a_{\text{max}} = -0.27$ . Such a large  $\alpha$ -value strongly suggestsa parameters that shift the observed spectrum in energy and fluxphotospheric origin of the emission during the analyzed time However, there exists a degeneracy in the current parametebin (Acuner et al. 2020). It is further natural to assume that the same emission mechanism operateshroughout a coherent 2019). Therefore, the whole pulse can be argued to be photosphericeven though most of the other time bins have nonthermal spectra ( $\alpha \sim -1$ ). As described in the introduction, these nonthermal spectra must then have been formed by subphotospheric dissipation (Ree& Mészáros 2005; Ryde et al. 2011) with RMSs as the most probable source of dissipation (e.g., Levinson & Bromberg 2008; Lundman &

In order to perform fast and efficient fits with the RMS proportional to the electron temperature (when the photon gainsnodel, we generate synthetic photospheric spectra over a large model as explained aboveWith the photospheric spectrave construct a table model in the Multi-Mission Maximum Likelihood Framework (3ML; Vianello et al2015). Here, we similarly but is a factor f lower in energy. The net effect is that include the broadening effect described in Section 3.3 by postprocessing of the spectraOur initial table model consists of 125 spectra.

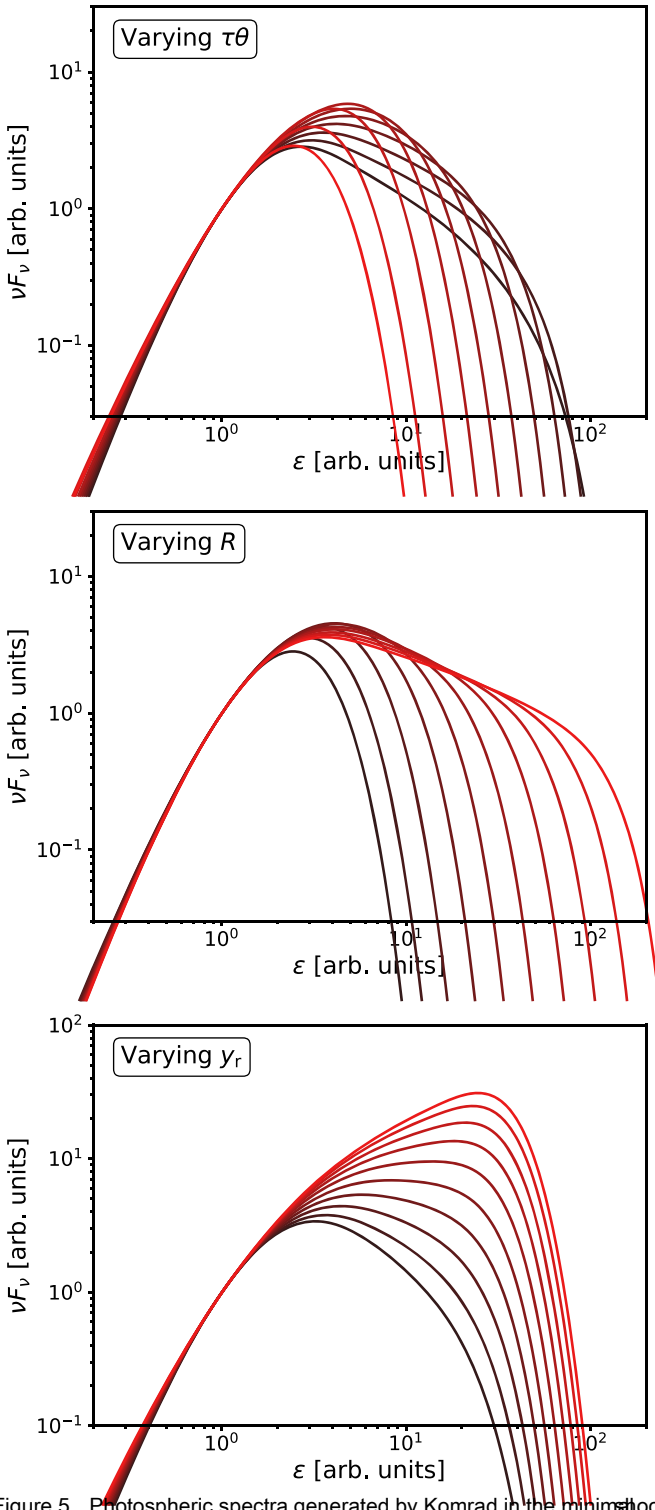


Figure 5. Photospheric spectra generated by Komrad in the minimulock model. In each panel, one of the three parameters τθς, and y is varied as indicated in the panels while the other two parameters are keptinstant. The constant parameter values are  $\tau\theta$  =  $\xi$  = 100, and y = 0.7. The value of the varying parameter increases from black to red, being evenly log-spaced from 50 for τθ, from 10 to <sup>2</sup> ftor R, and from 0.5 to 3 for lyncreasing τθ increases the thermalization. The ratio R determines the separation between the lower and upgave AIC = 1610 and can therefore equally well describe the cutoff in the spectrum, and determines the slope of the power-law segment. All data. The model parameters of the besit of the RMS model spectra have been normalized to unity in photon number 1(Nat ò = 1.

150314A with our RMS model. The data are from a narrow time bin at around 4.6 s after the trigger. The fit indicates that

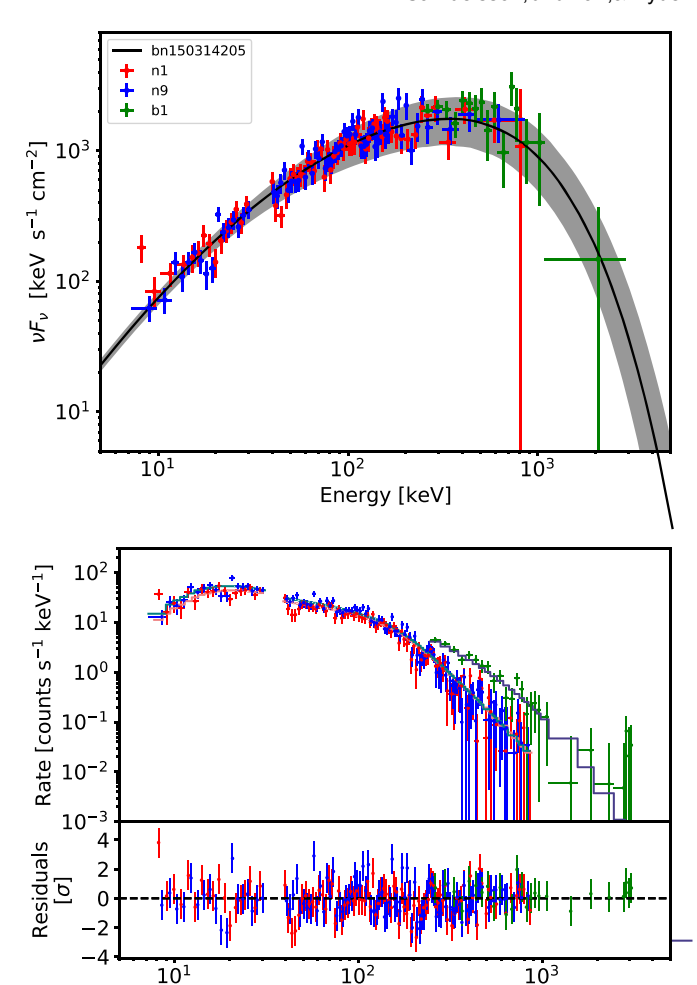


Figure 6. Time-resolved spectrum in GRB 150314A from a narrow time bin at around 4.6 s after the GBM trigger. Top panel: vF<sub>v</sub> spectrum of the best-fit RMS model. Two breaks are present around 30 and 400 keVThe best-fit model is depicted by the black line, and the gray region is its statistical uncertainty. The data points are derived from the counts fit and correspond to three of the triggered GBM detectors lote that the nonlinearity of the GBM response matrix meansthat the data points will not be accurate in a vFv spectrum; they are here shown only for visual purposes. Bottom panel: the bestfit model to the observed count data, including the residuals, which show random variationindicating a good fit.

Energy [keV]

there are two spectral breaks present, one at around 30 keV and the other at around 400 keV. The high-energy break corresponds to the energy the high-energy photons, those that reached the maximum energy  $_{\rm max} \sim 4q$  in the RMS, have downscattered to before decoupling. Conversely, the lowenergy break depends on how much the low-energy photons, those that entered the downstream with energy are heated by scatterings before they reach the photosphere (see also Section 5.1). A corresponding fit with the Band function yields  $\alpha = -0.73 \pm 0.06$  and a high-energy index  $\beta = -2.47 \pm 0.25$ , which are typical values for nonthermal spectra in GRBs (e.g., et al. 2016). Both the Band function and the RMS model are  $t\theta = 11.3 \pm 2.9$ , R = 290 ± 50, and y<sub>t</sub> = 1.72 ± 0.14. The initial separation between<sub>r</sub> and θ<sub>u</sub> was thus relatively large Figure 6 shows a fit to one of the nonthermal spectra in GRBand the thermalization moderate which allow for the broad,

nonthermal shape of the spectrum. The slope of the power-law segmentat around 200 keV reveals that uite a lot of energy

has been dissipated in the shockausing a large value of y Assuming a Lorentz factor of  $\Gamma$  = 300the parameters can be decoupled. This gives  $\theta = 0.055$  and  $\tau_i = 206$ . Translating this into the physical RMS parametersyields the upstream 4-velocity as  $\beta_u \gamma_u = 1.89$ , an upstream temperature of  $\theta_u = 8.81 \times 10^{-5}$ , and a photon-to-proton ratio of  $n_y/n_p =$  $2.01 \times 10^6$ . This fit thus illustrates that our model can be used to study the flow properties and the shock physics in observed GRBs.

#### Discussion and Conclusion

Dissipation in the optically thick regions of a GRB jethas the potential to generate a wide variety of released photosphericursts that have reported high-energy breaks aboysticuld spectralshapestherefore, it is a promising candidate for the prompt emission. Although RMSs are a natural dissipation paper, we have for the first time performed a fit to a timeresolved spectrum of the prompt emission in a GRB using an RMS model. This allowed us to determine the physical properties of the initial shock, such as its speed and the upstream photon temperature.

The main reason for the previous lack of fitted prompt spectra within an RMS framework is that RMSs are computationally expensive to simulate from first principles. To overcome this obstacle, we developed an approximate model (KRA; see Figure 1 for a schematic) based on the similarities between the bulk Comptonization of photons crossing an RMS and thermaComptonization of photons on hot electrons. By comparing the simulated spectra from Komrad, a code employing the KRA to those generated by a special relativistic radiation hydrodynamics code, we verified that the KRA can indeed accurately reproduce the RMS and downstream spectrafrom the full simulations in a wide parameter range (see Figures 2 and 3).

We connected the KRA to GRB prompt observations by creating a minimal shock model considering a single RMS shock is allowed to thermalize and cool adiabatically as it advects to the photosphere, where its radiation is released (sethat any early opticalemission is partof the afterglow. Early Figure 4 for a schematic). The model has only three free combined parameterτθ, which determines the amount of thermalization: R, which determines the extent the powerlaw segment; and y<sub>r</sub>, which determines the hardness ofhe power law (see Figure 5). Additionally, there are two postprocessing parameters for the normalization and the frequencyGiven that most optical observationsoccur quite late, they shift. We generated 125 spectra using the modeland, after accounting for broadening of the observed spectrum due to high-latitude effects and a radially varying photosphere, performed a fit to a broad spectrum in a narrow time bin of GRB 150314A as a proof of concept (see Figure 6).

### 5.1. Qualitative Spectral Features

Within the minimal shock modeldeveloped in this paper, there are some clear observational predictions. The spectra will consist of smooth low- and high-energy cutoffs, with a powerlaw segment in between. The low-energy cutoff is very smooth connection to the prompt emission in GRBs have been

there is an exponential cutoff at the highest energies. Typically, a single-break function is used to fit the spectral GRB data, e.g., the Band function, with its peak at Ep. Depending on the hardness of the power-law segmentcan correspond to either the low-energy cutoff (when y 1) or the high-energy cutoff (when  $y_r > 1$ ). Breaks both above and below the peak energy have been detectedditional breaks atlow energies (<10 keV) were reported in, e.g., Strohmayeret al. (1998), while additional high-energy breaksare discussed in, e.g., Barat et al. (1998). Within our model, bursts that have an additional low-energy break should be well fitted with an exponentialcutoff above Ep or very soft values of the highenergy power-law index  $\beta$  in the Band functionConversely, produce hard, low-energy slopes, as long as the smooth curvature is within the detector energy range. However, we mechanism, so far no such model has been fitted to data. In this ote that many of our generated spectra will appear as a single smooth curvature over a large range of energies (see, the best fit in Figure 6), due to the effects of thermalization on the downstream spectrumas well as the broadening effectsof high-latitude emission and radially varying emission.

> As it propagates toward the jet photosphere, the downstream spectrum will tend toward a Wien spectrum athe Compton temperatureThe more thermalized the downstream spectrum becomes the more difficult it will be to retrieve the original shock parameter Once the spectrum has relaxed into a Wien spectrum, the shock information is lost. This is an inherit degeneracy in photospheric models that is important to keep in mind when drawing conclusions abouthe physics from the parameter estimation.

## 5.2. Optical Emission

Although the curvature of the spectrum is very smooth, and although it may be outside the observable energy range of the prompt detectors, the Rayleigh-Jeans limit always exists in our spectra atow energies. Therefore, our minimal model with a occurring well below the photosphere. The downstream of the single shock cannot account for low-energy observations such as optical during the promptphase. Thus, we must conclude optical observations are rarand very few are within ~ 100 s parameters determining the shape of the released spectrum: thater trigger (see Oganesyan et al. 2021 for a recent example). Optical detections are commonly reported as prompt as long as they are observed within the  $\mathbb{T}_{90}$  of the GRB<sup>11</sup> (Yost et al. 2007; Klotz et al. 2009). This definition disregards whether the GRB had a quiescent period within the active phase ornot. could be the onset of the afterglow. This highlights the need for early optical observations in GRBswhich have the power to discriminate between the current models of the prompt emission (see also Oganesyan et al. 2019). Early optical observations also have the potenttal discern whether GRBs are significant contributors to the observed ultra-high-energy cosmic ray flux, as discussed in Samuelsson et al. (2019, 2020).

#### 5.3. Recollimation and Multiple Shocks

Recollimation shocks below the photosphere and their owing to the broadening effects discussed in Section 3.3, while investigated by several authors (e.g., Gottlieb et al. 2019). Although not discussed in this paper, we expect the KRA to be

 $<sup>^{10}</sup>$  The details of how  $\Gamma$  is related to the fitted parameters will be described in an upcoming paper which focuses on GRB data analysis using the KRA model.

 $<sup>^{11}</sup>$  The  $T_{90}$  is defined as the time during which 90% of the totalluence was detected from 5% to 95%.

able to model recollimation shocks as we Such shocks have (Lorentz factors are evaluated in the shock restrame), and different dynamics, but bulk Comptonization is still responsible subscriptsu and d indicate quantities in the upstream and for the energy dissipation, leading to the same spectral feature nownstream respectively. The ratio of pressure to density is that is, a power-law segment with a cutoff at high energies and given by

a Rayleigh-Jeansslope at low energies. Indeed, oblique shocks, such as recollimation shocks an be transformed into parallel shocks with a suitable Lorentz transformation (Henriksen & Westbury 1988). Therefore, a recollimation shock could plausibly be responsible for the subphotospheric dissipation in a GRB whose spectra can be wellfitted with the KRA.

The minimal shock model considered here consists a single RMS, dissipating energy over dynamical time. It is easy to imagine a more complex jet structure with multiple shocks and turbulence. However, although the dynamics belowthrough numerical integration of the spectrum inside the RMS the photosphere are complicated, it is not inconceivable that the end of dissipation. Furthermore  $\mathbb{I}_{u}=3a_{i}$ , given shape of a time-resolved spectrum is dominated by a single, strong dissipation even The good fit to the emission in GRB 150314A shows that the current minimal shock model can plausibly explain the data. Additional model complexity should energy by a facto $(r_d/r_u)^{1/3}$  (Blandford & Payne 1981). Using be considered only if the current model is found inadequate to Equation (A3), the increase can be written  $4 \frac{1}{3} \frac{1}{3}$ . The explain the observations. Further investigation will tell whether KRA cannot accountfor compression. Therefore, in order to the current minimal model is sufficient when applied to a largergenerate the same RMS spectrumthe codes need different sample of GRBs.

We acknowledge support from the Swedish National Space Agency (196/16) and the Swedish Research Council (Vetenskapsrådet,2018-03513).C.L. is supported by the Swedish National Space Board undegrant No. Dnr. 107/16. F.R. is supported by the Göran Gustafsson Foundation for Research ithe two codes get similar low-energy cutoff and average Natural Sciences and Medicine. This research made use of thedownstream energyAn additional equation is needed, which High Energy Astrophysics Science Archive Research Center (HEASARC) Online Service at the NASA/Goddard Space Flight Center (GSFC)In particular, we thank the GBM team for providing the tools and data.

### Appendix A Converting between the KRA Parameters and the RMS **Parameters**

In this appendix, we show how to convert between the Komrad parameters and the corresponding RMS parameters. The Komrad parameters are the upstream temperature the effective electron temperature in the shock zone and the Compton y-parameter the shock y. If one has obtained a value for the parameter τθ through a fit, then it is not possible to decouple  $\theta$  and  $\theta_{u,K}$  without additional information about the bulk Lorentz factor of the outflow. In that case, the final parameterswill be functions of the Lorentz factor. The radshock parameters are the upstream temperature<sub>1</sub>θ the upstream velocity in the shock rest frame and the photon to baryon density n/n p.

In the case of negligible magnetic fields and a radiationdominated equation of state, the relativistic shock jump conditions can be written as (e.g.,eloborodov 2017)

$$g_1(1 + W_0) = g_1(1 + W_0),$$
 (A1)

$$U_d(1 + W_d) + \frac{W_d}{4U_d} = U_u(1 + W_u) + \frac{W_u}{4U_u},$$
 (A2)

$$U_d r_d = U_u r_u, \tag{A3}$$

where  $w = 4p/pc^2$  is the dimensionlessenthalpy, p is the pressure  $\rho$  is the matter density,  $u \equiv \beta y$  is the four-velocity

 $W_d = \frac{4 \, \mathbb{I}_d m_e n_g}{3 m_o n_o},$ (A4)

$$W_{u} = \frac{4 \operatorname{Tu} m_{e} n_{g}}{3 m_{o} n_{o}}, \tag{A5}$$

where is the average photon energy measured in units of m and n/n p is equal in the upstream and the downstream in the case of a photon-rich shock. From Komrad, the is found that the upstream is a thermalized Wien spectrum.

Part of the energy gain across an RMS is due to plasma compression across the shockyhich increases the upstream upstream temperatures

$$q_{i, K} = q_i \left( \frac{\mu_u}{u_d} \right)^{1/3}. \tag{A6}$$

The jump conditions, together with Equation (A6), assure that relates the energy gain per scattering in the shock,  $\Delta \hat{o}/\hat{o}$ , between the two models The maximum photon energy in the shock roughly equals the relative energy gai $\mathbf{D}_{max} \sim \ \mathbf{D} \mathbf{I} / \mathbf{I}$ . In the radshock simulations, we empirically find that  $\mathbb{I}_{\max} \gg u_u^2 \ln(\mathbb{I}_d/\mathbb{I}_u)/x$ , where a constant value of  $\xi = 55$ works well across the parameterspace. In Komrad, the maximum energy is given by  $y_{max} = 4q$ . Therefore, we obtain

$$u_u^2 = x \frac{4q}{\ln(\mathbb{I}_d/\mathbb{I}_u)},\tag{A7}$$

where  $\xi = 55$ .

From a Komrad simulation, we know  $\theta_{u, K}$ ,  $\theta_r$ , and  $\mathbb{I}_d$ . Given the equation above, the system can be solved. Numerically, one can startby guessing ψ. Then, u<sub>u</sub> and θ<sub>u</sub> can be found from Equations (A6) and (A7). With Equations (A4) and (A5), the only unknown left is  $n_v/n_p$ , which can be solved from Equation (A1). If the original guess of u<sub>d</sub> was correctEquation (A2) should be satisfied.

If one wishes to instead go from the RMS parameters to the Komrad parameters, one can find w d and ud numerically through Equations (A1) and (A2),using Equations (A4) and (A5). Then  $\theta_{u,K}$  and  $\theta_r$  are found from Equations (A6) and (A7). The parameter y can be found iteratively by requiring that the downstream energyshould be equal in both models. In practice, a qualitative firstguess of y can be made from a

<sup>12</sup> Integration of the RMS zone instead of the downstream zone assures that there is no contamination from the shock formation history. The equations given here are valid for an RMS in steady statend to describe the average downstream energy from once the shock is in steady states the average downstream energy remains constamplanar geometry, the average photon energy in the steady-state RMS spectrum equals

plot of the RMS spectrum from radshock: by comparing the and power-law slope to the spectra in the bottom panel of Figure 5, the value of y can be estimated.

# Appendix B When Can the KRA Model Internal Shocks?

Consider a part of the jet that consists mainly of two masses: a slower and a faster mass with lab frame Lorentz factors  $\Gamma_1$ ? 1 and  $\Gamma_2$ ?  $\Gamma_1$ , respectively. The masses are assumed to be initially separated by a lab frame distance  $\delta r \square \delta l$ ,  $\delta l_2$ , where δl and δl are the corresponding initial lab frame widths of the slower and fastermass, respectively. The faster mass catches up to the slower mass  $\mathbf{z}\mathbf{t}$ dius $R_i \gg \mathbf{Z} + \frac{2}{1}\mathbf{d}$ . By then, the plasma between the masses has been highly compressed, increasing its pressureadiabatically until a forward and a reverse shock forms. The forward and reverse shocks propagate into the slower and faster masses espectively. The speed of the shocked region (i.e., the shared downstream, which is bounded by the forward and reverse shocks) is found by balancing the momentum flux in the rest frame of the shocked region,  $(\mathcal{F} \Gamma^2 h + p)$ , from both sides. Here  $h = \mathcal{F} e + p$  is the specific enthalpy, where p is the mass density and p is the of the unshocked masses. If we suppose that the initial pressurediation from both shocks sits inside plasma that opagates inside the two masses is small (such that h 3),den we can solve for the lab frame Lorentz factor  $\Gamma$  of the shocked material of only one shock is necessary.

$$G^2 \gg G_1 \mathcal{L} \frac{G_1 r_1^{1/2} + G_2 r_2^{1/2}}{G_1 r_2^{1/2} + G_2 r_1^{1/2}},$$
 (B1)

before being shocked. In a wide range of density ratios,  $(\mathbb{Q}/\mathbb{Q})^2 \ \square \ r_2/r_1 \ \square \ (\mathbb{Q}/\mathbb{Q})^2$  holds and the above expression can be simplified to

$$G^2 \gg G_1 \mathcal{L} \frac{f_2}{V_1}^{1/2}$$
 (B2)

The condition  $(G_2/G_1)^2 \square r_2/r_1 \square (G_1/G_2)^2$  also ensures that  $\Gamma_2$ ?  $\Gamma$ ?  $\Gamma_1$ . The radii where the two shocks have crossed their respective masses are then  $R_2 \approx 2\Gamma^2 \delta l_2$  and  $R_1 \gg Q_1^2 d_1$ , respectively. The masses are related to their widths and densities by δm ≈ 4<sup>2</sup>πρδl, and so the ratio of the radii where the reverse and forward shocks have crossed the respective masses can be written as

$$\frac{R_2}{R_1} \gg \left(\frac{r_1}{V_2}\right)^{1/2} \frac{d^{n_2}}{d^{n_1}}.$$
 (B3)

The relative Lorentz factors between the upstream (moving with Lorentz factor  $\Gamma_1$  and  $\Gamma_2$  for the forward and reverse shocks, respectively) and the downstream (Lorentz factor) give a measure of how relativistic the two shocks are. They carelloborodov A. M. 2010, MNRAS, 407, 1033 be computed using Equation (B2),

$$\overline{G}_{2} \gg \frac{G_{2}}{2G} \gg \frac{1}{2} \left( \frac{G_{2}}{G_{1}} \right)^{1/2} \left( \frac{f_{1}}{f_{2}} \right)^{1/4},$$
 (B4)

$$\bar{G} \gg \frac{G}{2G} \gg \frac{1}{2} \frac{f_2}{G} \left( \frac{r_2}{r_1} \right)^{1/2} \left( \frac{r_2}{r_1} \right)^{1/4},$$
 (B5)

and their ratio is

$$\frac{\overline{G}}{G} \gg \left(\frac{r_1}{r_2}\right)^{1/2}$$
 (B6)

The energy dissipated for each mass (in the rest frame of the shocked plasma) is » G - 1) dnc2, where G is the relative Lorentz factor between the up- and downstream, that

$$\frac{E_2}{E_1} \gg \frac{r_1}{r_2} \frac{d^{n_2}}{d^{n_1}} \gg \frac{R_2}{R_1}.$$
 (B7)

Based on the analysis above, we see that the collision of two masses with similar propertie $\delta m_1 \sim \delta m_2$  and  $\rho_1 \sim \rho_2$ , results in shocks of similar strengths,  $G \sim G$  The shocks also dissipate roughly the same amount energy,  $E_1 \sim E_2$ , and finish dissipating roughly at the same time, R₂. The heated radiation is located in the shared downstream between the two pressure, all of which are measured in the respective rest framehocks. Since the shocks have similar strengths and the heated with the same Lorentz factor (here called simply  $\Gamma$ ), modeling

The KRA can accurately model shocks as long as the relative energy gain per scattering is less than unity, ∆ò/ò □ 1.In Appendix A we found that  $D / \mathbb{I} = 0.018(g_{\mu} / \mathbb{I}_{b})^{2} \ln(\mathbb{I}_{b} / \mathbb{I}_{b})$ , which means that the approximation is valid up to \$3-4. Such a scenario is shown in Figure 3. For two blobs with  $\rho_1 \sim \rho_2$ ,  $\gamma_u \beta_u = 3$  translates to G » 3. Using Equations (B4) where  $\rho$  and  $\rho$  are the proper densities of the respective mass, and (B5), we find

$$\frac{G}{G}$$
  $\square$  36. (B8)

As an example, two masses of similar properties that propagate with initial Lorenz factors of  $\Gamma_1 \approx 50$  and  $\Gamma_2 \approx 1000$  would give rise to two RMSs with Δò/ò < 1, which can be modeled by the KRA.

#### ORCID iDs

Filip Samuelssom https://orcid.org/0000-0001-7414-5884 Christoffer Lundman https://orcid.org/0000-0002-0642-1055

Felix Ryde<sup>®</sup> https://orcid.org/0000-0002-9769-8016

#### References

Acuner, Z., Ryde, F., Pe'er, A., Mortlock, D., & Ahlgren, B. 2020, ApJ,

Ahlgren, B., Larsson, J., Nymark, T., Ryde, F., & Pe'er, A. 2015, MNRAS, 454, L31

Band, D., Matteson, J., Ford, L., et al. 1993, ApJ, 413, 281

Barat, C., Lestrade, J. P., Dezalay, J. P., et al. 1998, in AIP Conf. Ser. 428, Gamma-Ray Bursts, IV Hunstville Symposium,ed. C. A. Meegan, R. D. Preece& T. M. Koshut (Melville, NY: AIP), 278

Beloborodov, A. M. 2011, ApJ, 737, 68 Beloborodov, A. M. 2017, ApJ, 838, 125

Blandford, R. D., & Payne, D. G. 1981, MNRAS, 194, 1041

Bromberg, O., Mikolitzky, Z., & Levinson, A. 2011, ApJ, 733, 85

Chang, J., & Cooper, G. 1970, JCoPh, 6, 1

Dereli-BéguéH., Pe'er,A., & Ryde, F. 2020, ApJ, 897, 145

```
Golenetskii, S. V., Mazets, E. P., Aptekar, R. L., & Ilinskii, V. N. 1983, Natur,
  306, 451
Gottlieb, O., Levinson, A., & Nakar, E. 2019, MNRAS, 488, 1416
Henriksen, R. N., & Westbury, C. F. 1988, ApJ, 327, 50
Ito, H., Levinson, A., & Nakar, E. 2020, MNRAS, 499, 4961
Ito, H., Levinson, A., Stern, B. E., & Nagataki, S. 2018, MNRAS, 474,
  2828
Klotz, A., Boër, M., Atteia, J. L., & Gendre, B. 2009, AJ, 137, 4100
Levinson, A. 2012, ApJ, 756, 174
Levinson,A. 2020, PhRvE, 102, 063210
Levinson, A., & Bromberg, O. 2008, PhRvL, 100, 31101
Levinson, A., & Nakar, E. 2020, PhR, 866, 1
Li, L., Ryde, F., Pe'er, A., Yu, H.-F., & Acuner, Z. 2021, ApJS, 254, 35
López-Cámara, D., Morsony, B. J., Begelman, M. C., & Lazzati, D. 2013, ApJ,
López-CámaraD., Morsony, B. J., & Lazzati, D. 2014, MNRAS, 442, 2202
Lundman, C., & Beloborodov, A. M. 2019, ApJ, 879, 83
Lundman, C., & Beloborodov, A. M. 2021, ApJL, 907, L13
Lundman, C., Beloborodov, A. M., & Vurm, I. 2018, ApJ, 858, 7
Lundman, C., Pe'er, A., & Ryde, F. 2013, MNRAS, 428, 2430
Nakar, E., & Sari, R. 2012, ApJ, 747, 88
```

```
OganesyanG., Karpov, S., Jelínek, M., et al. 2021, arXiv:2109.00010
OganesyanG., Nava, L., Ghirlanda, G., Melandri, A., & Celotti, A. 2019,
   A&A, 628, A59
Pe'er, A. 2008, ApJ, 682, 463
Rees,M. J., & Mészáros,P. 2005, ApJ, 628, 847
Rybicki, G. B., & Lightman, A. P. 1979, Radiative Processes in Astrophysics
   (New York: Wiley)
Ryde, F., Lundman, C., & Acuner, Z. 2017, MNRAS, 472, 1897
Ryde, F., Pe'er, A., Nymark, T., et al. 2011, MNRAS, 415, 3693
Samuelsson, Bégué, D., Ryde, F., & Pe'er, A. 2019, ApJ, 876, 93
SamuelssonF., Bégué, D., Ryde, F., Pe'er, A., & Murase, K. 2020, ApJ,
   902, 148
Strohmayer, T. E., Fenimore, E. E., Murakami, T., & Yoshida, A. 1998, ApJ,
   500,873
Vianello, G., Gill, R., Granot, J., et al. 2018, ApJ, 864, 163
Vianello, G., Lauer, R. J., Younk, P., et al. 2015, arXiv:1507.08343
Vurm, I., & Beloborodov, A. M. 2016, ApJ, 831, 175
Wheaton,W. A., Ulmer, M. P., Baity, W. A., et al. 1973, ApJL, 185, L57
Yost, S. A., Aharonian, F., Akerlof, C. W., et al. 2007, ApJ, 669, 1107
Yu, H.-F., Dereli-BéguéH., & Ryde, F. 2019, ApJ, 886, 20
Yu, H.-F., PreeceR. D., Greiner, J., et al. 2016, A&A, 588, A135
```